

## Article

# Crystal Structure of a New 1:1 Acridine-Diclofenac Salt, Obtained with High Yield by a Mechanochemical Approach

Artur Mirocki <sup>1</sup>, Eleonora Conterosito <sup>2</sup>, Luca Palin <sup>2,3</sup>, Artur Sikorski <sup>1</sup>, Marco Milanesio <sup>2</sup>  
and Mattia Lopresti <sup>2,\*</sup>

<sup>1</sup> Faculty of Chemistry, University of Gdansk, W. Stwosza 63, 80-308 Gdansk, Poland

<sup>2</sup> Dipartimento di Scienze e Innovazione Tecnologica, Università del Piemonte Orientale, Viale T. Michel 11, 15121 Alessandria, Italy

<sup>3</sup> Nova Res s.r.l., Via D. Bello 3, 28100 Novara, Italy

\* Correspondence: mattia.lopresti@uniupo.it

**Abstract:** The liquid-assisted grinding (LAG) approach was exploited to efficiently produce a new salt cocrystal with a minimum expenditure of reagents and energy, with possible application in the pharmaceutical field. LAG was applied to the acridine/diclofenac couple, and a new cocrystal was obtained with a 1:1 ratio of reagents and its structure resolved by X-ray powder diffraction (XRPD). The XRPD analysis confirmed that the yield is higher than 90% and the limited use of solvents and the absence of waste generally makes the synthesis very efficient and with the minimum possible environmental impact. The crystal structure of the title compound was compared to a previously solved 1:2 cocrystal, also with the aid of Hirshfeld's surface analysis and calculations of the energy framework. The packing of the 1:1 structure is stabilized by a strong H-bond and partial  $\pi \cdots \pi$ -stacking interactions. It differs considerably from that of the previously identified cocrystal, in which two strong hydrogen bonds and a perfect interlocking of the molecules thanks to the  $\pi \cdots \pi$  stacking induce a much higher stability, as confirmed by energy framework calculations. DSC analysis confirmed its purity and a melting point at 140 °C, which is different from those of the two reactants.

**Keywords:** API salt cocrystal; acridine; diclofenac; LAG; high yield synthesis; crystal packing; hirshfeld analysis; DSC



**Citation:** Mirocki, A.; Conterosito, E.; Palin, L.; Sikorski, A.; Milanesio, M.; Lopresti, M. Crystal Structure of a New 1:1 Acridine-Diclofenac Salt, Obtained with High Yield by a Mechanochemical Approach. *Crystals* **2022**, *12*, 1573. <https://doi.org/10.3390/cryst12111573>

Academic Editors: José Gavira, Fiora Artusio and Rafael Contreras-Montoya

Received: 8 October 2022

Accepted: 1 November 2022

Published: 4 November 2022

**Publisher's Note:** MDPI stays neutral with regard to jurisdictional claims in published maps and institutional affiliations.



**Copyright:** © 2022 by the authors. Licensee MDPI, Basel, Switzerland. This article is an open access article distributed under the terms and conditions of the Creative Commons Attribution (CC BY) license (<https://creativecommons.org/licenses/by/4.0/>).

## 1. Introduction

One of the new strategies used in modern medicinal chemistry is to obtain active pharmaceutical ingredients (APIs) in the form of multi-component crystals, in different ratios and/or in salt or solvated form. At the same time, X-ray powder diffraction can now be exploited to solve crystal structures obtained only in microcrystalline form as often occurs in LAG conditions [1]. Such an approach allows obtaining new forms and structural data that can be used to rationally design drugs with improved physicochemical properties and pharmacological performances [2–7]. An excellent example is diclofenac (IUPAC: 2-(2-(2,6-dichloroanilino)phenyl)acetic acid), a fast-acting non-steroidal anti-inflammatory drug with antipyretic and analgesic properties, used for various inflammations, degenerative joint disease, and also after surgery [8–14]. A search of the Cambridge Structure Database (CSD version 5.43, update March 2022) [15] showed that ca. 100 crystal structures of multi-component crystals involving this API were determined using single-crystal X-ray diffraction (SCXRD), involving pyrazoles, clofazimine, norfloxacin, fenamates, proline, sulfamethazine, and others [16–21]. Among them, an extensive structural study allowed obtaining molecular crystals of diclofenac with acridines by the slow evaporation of different solvents [22]. In this paper, a salt cocrystal of acridine with diclofenac (1:2 stoichiometry) and a solvated salt of ethoxyacridine with diclofenac are described. The most common way to obtain multi-component crystals involving APIs is solution crystallization. However,

this technique is associated with many problems such as low purity, but also the large-scale use of solvents (and thus wastes) and energy if heating is needed for the API solubilization. Moreover, the possibility of obtaining different polymorphs, solvates, or crystals with stoichiometric diversity of reagents is possible [23,24], but sometimes some cocrystals can be obtained only by changing the preparation method. Bearing in mind that liquid-assisted grinding (LAG) enables producing of molecular crystals, e.g., cocrystals involving diclofenac [25], as well as acridines [1], the LAG approach was applied to obtain new molecular crystals involving acridine/diclofenac couple. As a result, a new acridine:diclofenac (1:1 stoichiometry) cocrystal was obtained and its structure was solved using the XRPD method using the sample obtained by LAG without any recrystallization. The crystal structure of the title compound was compared with that of the 1:2 cocrystal, previously determined by the single crystal X-ray diffraction method [22]. Hirshfeld surface analysis and energy framework calculations were also performed. Additionally, DSC analysis on the cocrystal and mechanical mixture of reactants was carried out to shed light on the thermal behavior of the newly obtained cocrystal, in comparison with the mechanical mixture. To the best of our knowledge, the crystal structure of the title compound is the first structure of multi-component crystals involving diclofenac determined using the XRPD method deposited within the CCDC.

## 2. Materials and Methods

### 2.1. Solid State Synthesis

All of the chemicals were purchased from Merck (Sigma-Aldrich, St. Louis, MO, USA). An extensive investigation of the possible molar ratios between the acridine and the diclofenac in the asymmetric unit was carried out as in our previous work [1]. In addition to different reagent ratios, the type of liquid medium for the mechanochemical reaction was varied, spanning from pure water to pure ethanol and including a 50:50 mixture of the two. The exploration was carried out taking into account that it is possible to obtain different cocrystals based on the variations of the type of solvent, as reported in the scientific literature [26,27]. A 1:1 molar ratio of the reactants was then extended up to a 1:2, as in the single-crystal structure already reported in the literature [22], to investigate the possibility of obtaining such a complex also by LAG, but without any results. Different methods (all in one and multistep) of solvent addition before grinding were tested to select the one with the highest yield. In the final recipes, acridine (0.06 g, 0.334 mmol) and diclofenac (0.093 g, 0.314 mmol) were ground in a ceramic mortar together with 10 drops (about 0.4 mL) of ethanol three times (each grinding 3 min), then treated in an oven at 93 °C for 3 h to obtain a dried and well-crystallized sample. The same procedure was used to obtain molecular crystals of 9-aminoacridine with diclofenac, since a single crystal was obtained [22]. However, these attempts were unsuccessful, as in the case of 9-aminoacridine with naproxen [1].

### 2.2. X-ray Powder Diffraction and Structure Solution

A Bruker D8 Advance diffractometer equipped with a LynxEye XE-T detector and Cu  $K_{\alpha}$  ( $\lambda = 1.5418 \text{ \AA}$ ) radiation was exploited for the XRPD data collection. The instrument has a goniometer radius set to 280 mm and the tube was set at 40 mA current and 40 kV electric potential. The diffractometer was operated in two different configurations, the first consisting of an auto-sampler setup in Bragg–Brentano geometry to analytically track the correct execution of the mechanochemical reaction and the possible presence of residual reagents inside the reaction products. On top of the sample an air scatter knife was positioned to reduce noise during low angle measurements. Soller slits of 2.5° were used on both primary and secondary optics to reduce axial divergence. Variable diverging slits were used as primary optics to ensure a constant sample irradiation of 17 mm. The diffraction patterns were collected in an angular range from 3° to 70° in  $2\theta$  with a step size of 0.01° and irradiation time 0.05 s/step. The second setup is a capillary stage with Debye–Scherrer geometry that was used for data collection for structure solution. A Göbel mirror with

a 1 mm focusing hole was used as the primary optic together with a planar 0.6 mm slit. The sample was positioned in a 0.7 mm glass capillary and measured in order to obtain an optimal angle resolution suitable for indexing the reaction product. The measurement was carried out in a  $2\theta$  range of  $3^\circ$  to  $70^\circ$ , a step-size of  $0.005^\circ$  and exposure time of 5 s, resulting in 18 h of data collection. The new structure was indexed by EXPO2014 [28] and solved exploiting simulated annealing in direct space with the same software. The final structure refinement was carried out by Topas Academic [29,30] on both flat and capillary samples. To facilitate the indexing and structure solution and simulate at best a 100% pure phase pattern, the reactant residual main peaks were removed. Additionally, it is worth noting that the structure solution was carried out taking into account many possible unit cells and lattices and afterward possible solutions and crystal packing. The indexing was carried out independently using the EXPO and Topas softwares and the final lattice parameters and space groups were selected by looking to the agreement factor and absence of non-indexed peaks (excluding non-reacted acridine and diclofenac peaks). Moreover, a contact analysis was carried out and the possibly acidic H position obtained by energy framework calculations to support the chosen solution. For the sake of completeness, quantitative phase analysis was then performed with the complete pattern to further confirm the obtained structure and estimate the excess of reactants in the final structure pattern and thus the yield. Such an analysis was carried out according to the Rietveld method of multi-structural refinement, as described in section A2 of the article by Lopresti et al. [31], and allowed also an improvement of the agreement factor between the calculated and experimental patterns. Several polymorphs of acridine and diclofenac were tested and in the final refinement, the fitting of all of the observed peaks was possible with one acridine and two monoclinic different forms of diclofenac. Such a refinement suggested 92% of the 1:1 title compound, 3.5% of acridine, and a 4.5% of diclofenac.

### 2.3. Thermal Analysis

DSC analyses were performed using a DSC 3 instrument from Mettler Toledo. Profiles were collected in the range from 35 to 200 °C in an air atmosphere with a ramp of 5 °C/min and back to RT. The samples and reference were positioned in an aluminium 40  $\mu$ L flat sample pan with a same-material lid.

### 2.4. Hirshfeld Surface and the Energy Frameworks Ab Initio Calculations

All of the ab initio calculations of the Hirshfeld surfaces, fingerprint plots, and energy frameworks were carried out by using CrystalExplorer 17.5 [32]. For both structures, the Hirshfeld surfaces were calculated with a high-resolution setting. Each molecule's wavefunctions and pairwise interaction for the energy framework estimation were calculated using Tonto [33] with the B3LYP DFT method by employing the 6-31 G(d,p) basis set, as implemented in CrystalExplorer. The scale for the tube size employed for energy framework pictures was 80 and the cut-off value for energies was set to 0  $\text{kJ}\cdot\text{mol}^{-1}$ . Calculations of the interaction energies between each molecule and the chemical neighborhood were performed. From the results, the sum of the lattice energy for each individual molecule was obtained as one half the product of the number of symmetry-equivalent molecules in the cluster and the total energy, as reported in Thomas et al. [34]. Mercury 2022.1 CSD release was used to assess the presence of voids [35].

## 3. Results and Discussion

### 3.1. Structure Solution by X-ray Powder Diffraction and DSC Analysis

The synthesis of the cocrystal was carried out using the mechanochemical approach, as described in the previous section. The LAG was performed manually for a few minutes, and afterward the synthesis product was dried in an oven to remove the solvent molecules. The obtained sample was at first measured in the flat sample geometry, where the presence of a new cocrystal was assessed, to optimize the yield so as to obtain the final recipe with an estimated yield of about 92%. This yield was obtained by the XRPD pattern

(Figure 1c), showing four reflections belonging to the reactants ( $9.37^\circ$ ,  $15.26^\circ$ ,  $21.41^\circ$ , and  $23.84^\circ$  in two theta), which were quantified globally as 8% in weight (3.5% of acridine, 4.5.0% of two polymorphs of diclofenac). Given the nature of the synthesis process, it was not possible to grow a single crystal large enough for structural resolution. For this reason, the resolution attempt was performed using XRPD. The sample was then placed in a 0.7 mm glass capillary for a XRPD analysis in Debye–Scherrer geometry to obtain optimal peak sharpness, avoiding or limiting peak superposition. After the data collection, the indexing and the subsequent resolution by simulated annealing were carried out using EXPO2014 software [28]. In both procedures, the four reflections of the reactants were excluded. The product crystallizes in the monoclinic system, with the  $P2_1/n$  space group. Cell parameters are:  $a = 22.7175(9)$  Å,  $b = 11.4960(5)$  Å,  $c = 8.6040(3)$  Å,  $\beta = 90.53554(2)^\circ$ . The volume of the unit cell is  $2246.93$  Å<sup>3</sup>. In the asymmetric unit (Figure 1a), the ratio between the reagents is retained, resulting in a one-to-one ratio between acridine and diclofenac. The crystal packing of the new structure (Figure 1b) was compared to the one previously identified in the work of Mirocki and Sikorski [22]. Whereas in the previously solved structure, the driving force for the crystallization was the formation of strong charge-assisted hydrogen bonds and of the perfect  $\pi$ -stacking between acridine and diclofenac, in the new product only one hydrogen bond is present and the ring substituted with the acidic function is positioned perpendicularly to the acridine rings (Figure 1b) with much fewer degrees of  $\pi$ - $\pi$  interaction. This is attributed to the short reaction time that is involved in the formation of the 1:1 product by the LAG method: with longer crystallization times, such as those attained by solution crystallization, diclofenac molecules overcome the steric hindrance assuming a planar conformation. The result is a more energetically advantageous packing that fully exploits the  $\pi$ -stacking between diclofenac and acridine, maximizing the hydrogen bonds among diclofenac and acridine molecules. In Figure 1c the structural Rietveld refinement performed on the pattern collected by powder diffraction is reported. For a more accurate result, the refinement in the figure was carried out by fitting at the same time the new structure and those of the residual reagents, as detailed in the experimental section. Only one small peak is calculated at the position  $21.4^\circ$  in 2 theta, but it was not well-fitted, probably because of the low amount and the disorder of the corresponding phase. The index of agreement between the calculated and the experimental pattern is  $R_{wp} = 7.959$ . The likelihood of the 1:1 crystal structure together with the visual good fit (Figure 1c) and  $R_{wp}$  suggest that the packing is correct.

The typical limitations of X-ray diffraction, exacerbated by peak superposition and the limited resolution of the mandatory powder diffraction approach, render impossible a correct location of the H atom (bonded to the N atom of acridine or O atom of diclofenac) and thus the neutral or salt form of the cocrystal. The small pKa difference and the use of the neutral form of diclofenac suggests a neutral cocrystal, but as suggested by [36], the proton exchange from O to N can be facilitated by the absence of an energy barrier and by the very similar relative energy of the two minima. Moreover, the hydrogen can be in straight configuration, pointing directly to the nitrogen or bent as suggested by the Rietveld refinement. The three possible configurations are depicted in Figure 2. An experimental proof of the hydrogen location is tough or impossible, since N-H and O-H infrared bands have similar position and shape [37]. NMR is also rather complicated to be applied to the H position determination in the solid state. For these reasons, to discriminate among these three possible configurations, they were explored using energy framework calculations, whose description is carried out in a dedicated section.

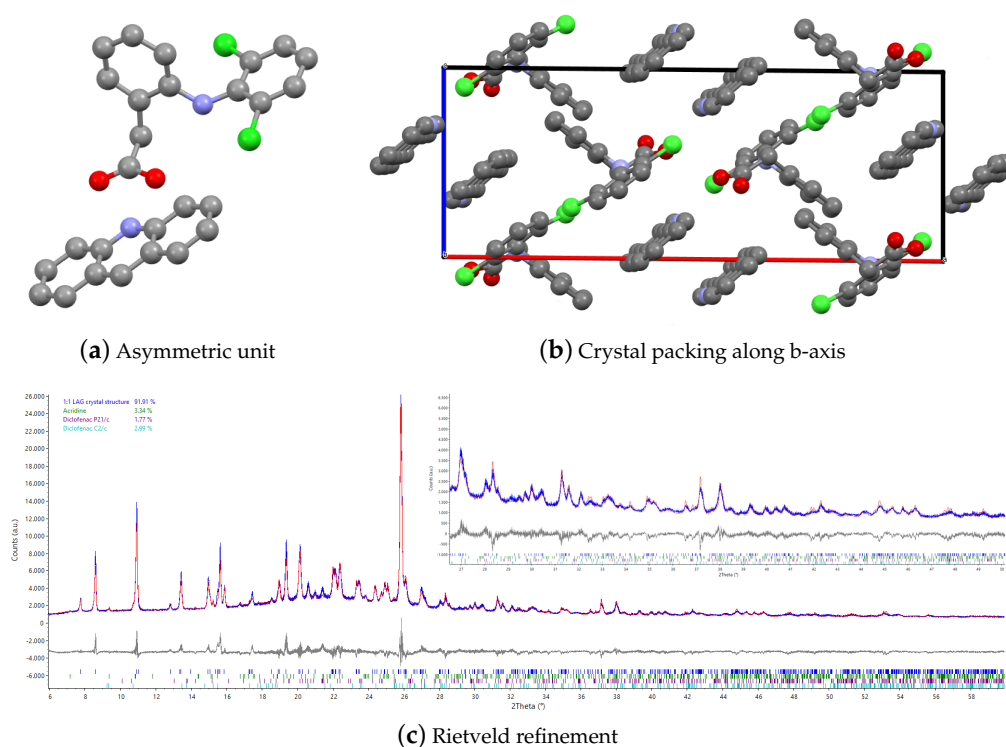


**Figure 1.** (Top): asymmetric unit (left) and crystal packing (right) of the new cocrystal; (Bottom): Rietveld refinement of the new structure.

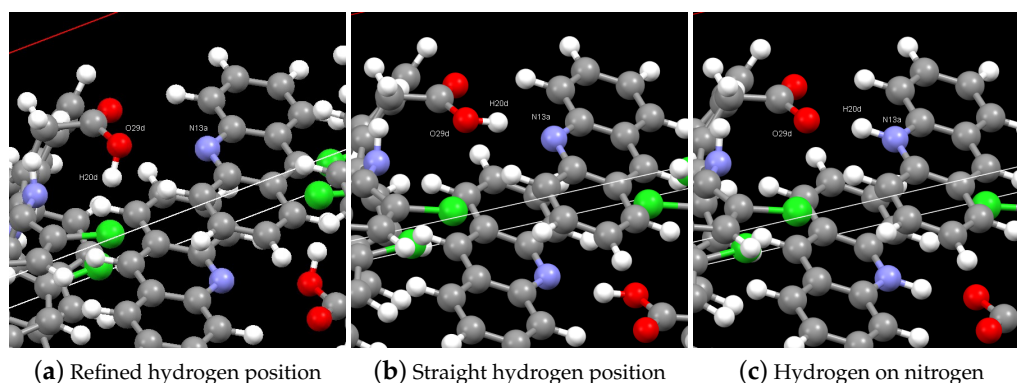


**Figure 2.** The three different hydrogen configurations studied.

### 3.2. Thermal Analysis

To give a final proof of the presence of a new crystalline cocrystal and further explore the thermal behavior and stability of the 1:1 form, DSC was used to measure the melting temperature of both the LAG reaction product and a unreacted mechanical mixture of acridin and diclofenac in the same molar ratios, and the effect of cooling on the sample crystallinity. In Figure 3 the black curve refers to the DSC of the title cocrystal. During heating, a single-phase transition peak is shown at 140 °C, which is much closer to acridine (m.p. about 100 °C)

than diclofenac (m.p. 284 °C). During cooling no crystallization peak was observed, meaning that the cocrystal does not return to the two individual chemical species, but remains an amorphous solid. On the contrary, the mechanical mixture has a single melting peak at 106 °C and a crystallization homologous at 84 °C, which correspond to the thermal neighborhood in which the melting and crystallization of acridine are expected, as reported in the literature [38]. This indication confirms that the drying process at 93 °C is below the

melting of acridine alone (about 100 °C from the literature) and in the mechanical mixture (106 °C). In Figure 3, the melting point of diclofenac is not observed, as it occurs at 285 °C, a temperature where melting can be sidled by partial decomposition. However, the crystallization of acridine in the mechanical mixture cooling from 200 °C is sufficient, not only to prove that the obtained structure has high purity and has a different melting point, but also to demonstrate that the mechanical mixture is thermally stable up to 200 °C and does not react even at high temperatures in the presence of melted acridine. Interestingly, in the similar case of acridine/naproxen [1], the melting point of the 1:1 form was smaller than the two reactants, while in this case the 1:1 acridine/diclofenac cocrystal melts above 140 °C, whereas the mechanical mixture starts melting at 106 °C indicating an increase of about 40 °C in its melting point, suggesting an improved thermal stability of its solid form.

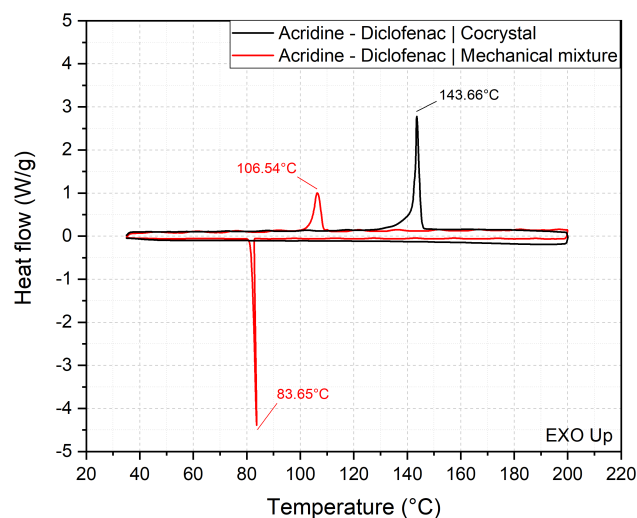


**Figure 3.** DSC curve of the novel cocrystal structure (black) compared to the one relative to the simple mechanical mixture of acridin and diclofenac (red).

### 3.3. Hirshfeld Surface Calculations

To extend the understanding and highlight the differences between the new structure obtained by LAG and the single-crystal resolved one by Mirocki and Sikorski [22], *ab initio* calculations of the Hirshfeld surface and energy frameworks were performed on both 1:1 and 1:2 cocrystals. Moreover, the calculations for the 1:1 case were repeated in three possible cases depicted in Figure 2 to assess the best H location according to the energetic viewpoint. In Figure 4 the shape index plotted on the Hirshfeld surface of an acridine of the 1:2 single crystal structure is reported. Alternating red and blue triangles on the surface indicate the presence of a  $\pi$ -stacking interaction. As a result, the acridine within the surface in Figure 4 is perfectly interlocked by the surrounding net of diclofenac and acridine molecules, bonded by medium–strong hydrogen bonds, one of them charge-assisted. Conversely, in the short time of a LAG reaction and the quasi-solid conditions, diclofenac is not able to overcome the energetic barrier to assume a planar conformation, resulting in a only partial  $\pi$ -stacking between acridine and the chlorine-substituted ring of diclofenac (Figure 1b). For these considerations, the 1:2 single crystal cocrystal appears more stable than the 1:1 LAG one. The same effect can be observed on both faces of the molecule, hinting that the close packing of the structure is mostly driven by a  $\pi$ - $\pi$  interaction. To better analyze the packing of the 1:1 crystal structure and exclude the neglect of water or ethanol coming from the used LAG solution, the voids within the structure were calculated by mercury. For this operation a standard size probe set at 1.2 Å was used to simulate a water molecule. Following this calculation, there are no solvent accessible voids and therefore the crystal packing depicted in Figure 2 does not contain either free solvent or pores large enough for solvent to be adsorbed inside.

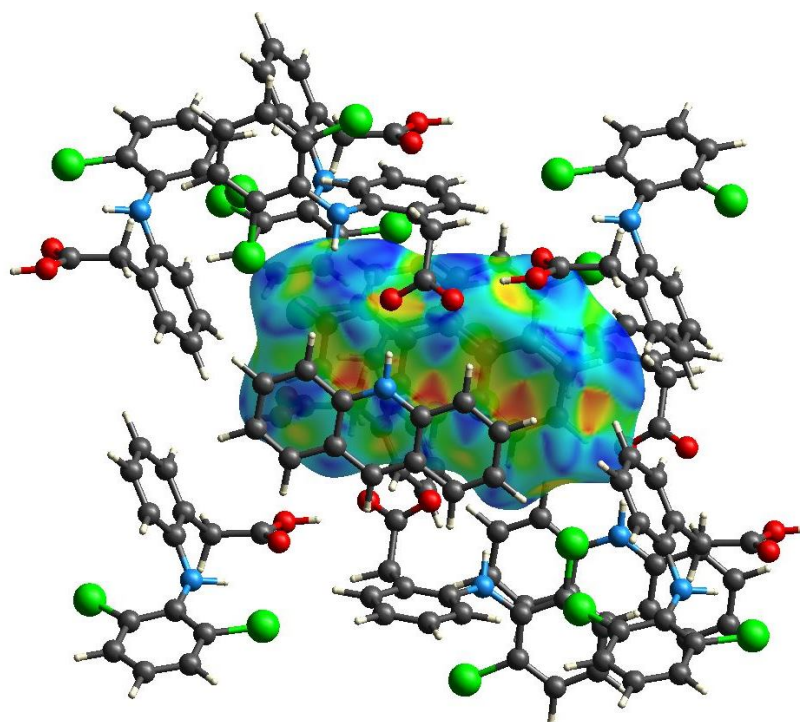


**Figure 4.** Shape index plotted on the Hirshfeld surface for the 1:2 single-crystal structure.

In Figure 5, the calculations of the energy frameworks with their coulomb and dispersion contributions are reported separately. As regards the Coulomb energy frameworks, it is evident that the electrostatic effects are not conjugated in an expanded network, but in local chair-shaped clusters that are oriented head–tail with those parallel along the *c*-axis. A different behavior is observed for dispersion energy frameworks in which a 2D network exist along the *b*–*c* plane, but it is not connected along the *a*-axis. Figure 5a also shows the energy frameworks belonging to the lattice destabilization forces (yellow cylinders). These appear to be very small in size, a sign that from the simulations of the energy frameworks the structure has high stability. This is further verified by the calculation of the total lattice energy, which turns out to be  $-605.9 \text{ kJ}\cdot\text{mol}^{-1}$ .

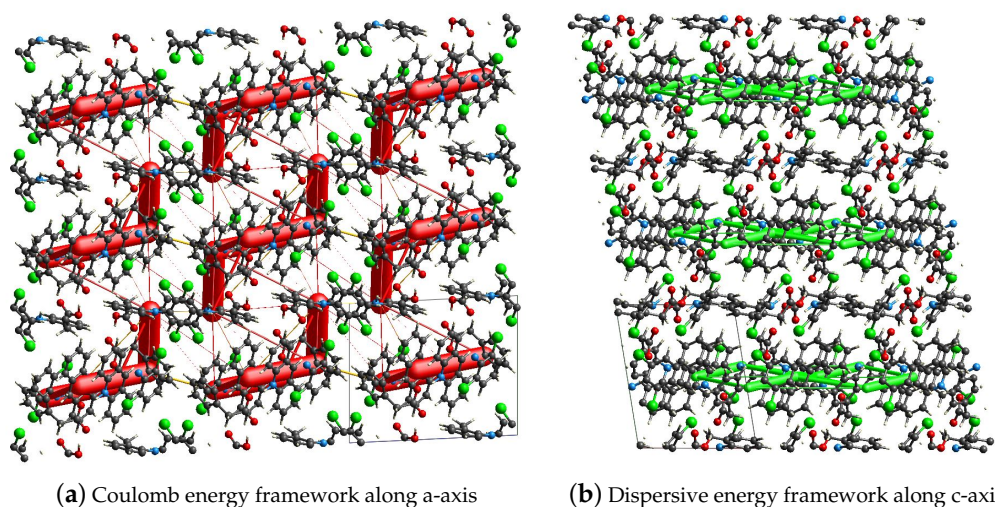


**Figure 5.** Energy frameworks calculated for the 1:2 single crystal-solved structure.

Figure 6 shows the shape index plotted on the Hirshfeld surface for comparison with Figure 4. The alternating red and blue triangles (resulting by the presence of  $\pi$ -stacking) are observed only in the overlap between acridine and the chlorine-substituted ring of

diclofenac. The second ring of diclofenac is instead positioned so as to be perpendicular to the acridine plane, which results in a less efficient stacking than that observed in the single-crystal resolved structure. However, this orientation allows a stabilization by the means of a hydrogen bond that is established between the carboxylic function and the heteroatom of the acridine.

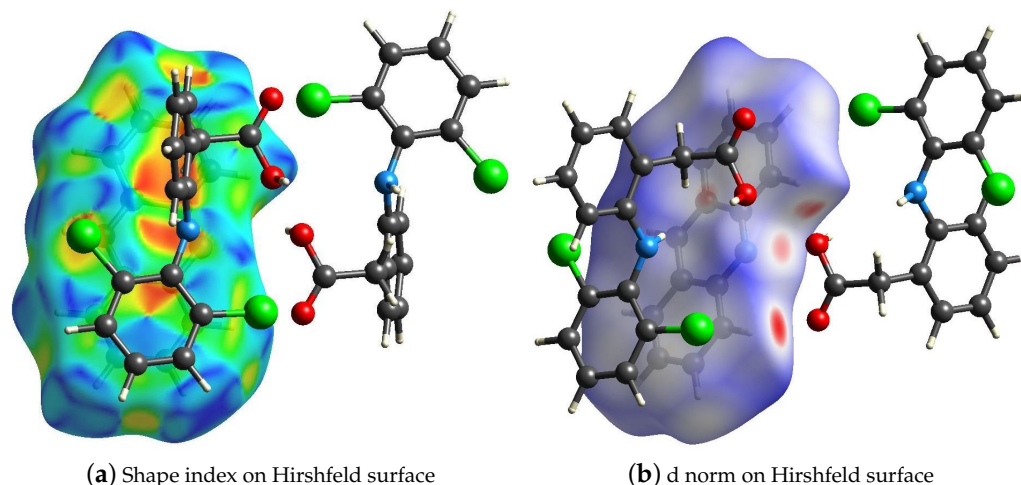


**Figure 6.** Hirshfeld surface for the LAG 1:1 structure.

In Figure 6b the unconventional position of the hydrogen of the carboxylic function of diclofenac can be observed. During the structural resolution, and in the later refinements, the hydrogen was always moved iteratively to a final position where hydrogen is not oriented towards nitrogen of acridine. To have a better understanding of the true orientation of hydrogen, two neutral possible structures were produced: one with the hydrogen oriented as suggested by the Rietveld refinement (Figure 2a) and the second with the hydrogen with a forced position that makes it oriented towards the nitrogen of acridine (Figure 2b). A third structure, consisting of the salt form with the hydrogen bonded to the N atom of the acridine to form the acridinium cation, was also produced (Figure 2c). On the three structures, the Hirshfeld surface was calculated and the fingerprint plots of the H-N (or H-O for the acridinium) interaction are reported in Figure 7. In the fingerprint plots of Figure 7b,c,  $d_e$  and  $d_i$  distances belonging to the bonds N-H and O-H, respectively, are equivalent. This confirms the hypothesis that the structure can host a proton transfer effect, probably associated with pH variations. The fingerprint of the structure giving the best agreement after Rietveld refinement (Figure 2a) indicating a weak or no H-bond interaction (absence of the spike) suggests that this configuration is wrong. The hydrogen must therefore be located along the  $N \cdots O$  direction with a strong H bond in the neutral (H on O atom) or salt (H on N atom) form. The corresponding Hirshfeld fingerprint (Figures 2b and 7) suggest in both cases a strong H-bond interaction (more directional with a more marked spike in Figure 2b of the neutral form), but it is not enough to chose the best H location. Energy framework calculations were then used to assess the best solution. The analysis of the contacts indicates that the three possible configurations have the following total lattice energies:  $-159.9 \text{ kJ}\cdot\text{mol}^{-1}$  (refined hydrogen position structure Figure 2a),  $-215.2 \text{ kJ}\cdot\text{mol}^{-1}$  (neutral form with hydrogen pointing to N atom as in Figure 2b) and  $-513.4 \text{ kJ}\cdot\text{mol}^{-1}$  (salt form with H on the N atom as in Figure 2c). These data allow us to select the salt form as the most stable one among the three possibilities and consequently it was chosen to be deposited in the CCDC database.

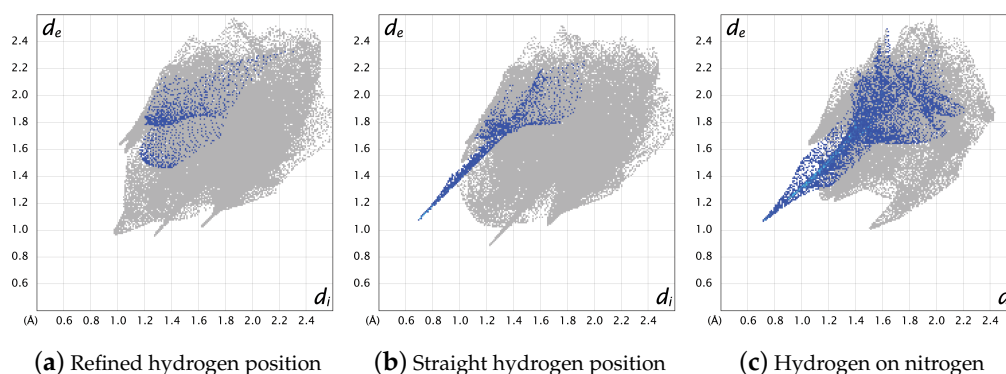


**Figure 7.** Fingerprint plots with the highlighted H-N interactions (a,b) and H-O (c) for the three different configurations assumed by the hydrogen, in the LAG-solved 1:1 structure, as in Figure 2.

Figure 8a shows the energy framework given by the electrostatic effects of the structure. The size of the cylinders gives a hint about the contribution to the total lattice energy, which is still very high and comparable to the single crystal form of the cocrystal. As previously observed in Figure 5a, the energy framework still does not present a full 3D conjugation, but local L-shaped clusters. In Figure 8b it can be observed how the contribution of the dispersion forces to the stabilization of the lattice still presents larger and smaller cylinders, but the differences in size are much smaller than the ones between the Coulomb forces. Moreover, dispersion forces are connected along the entire structure. The combination of all of the effects is however much less efficient in stabilizing the lattice than that observed for the single-crystal resolved cocrystal, with a lattice energy equal to  $-513.4 \text{ kJ}\cdot\text{mol}^{-1}$ .

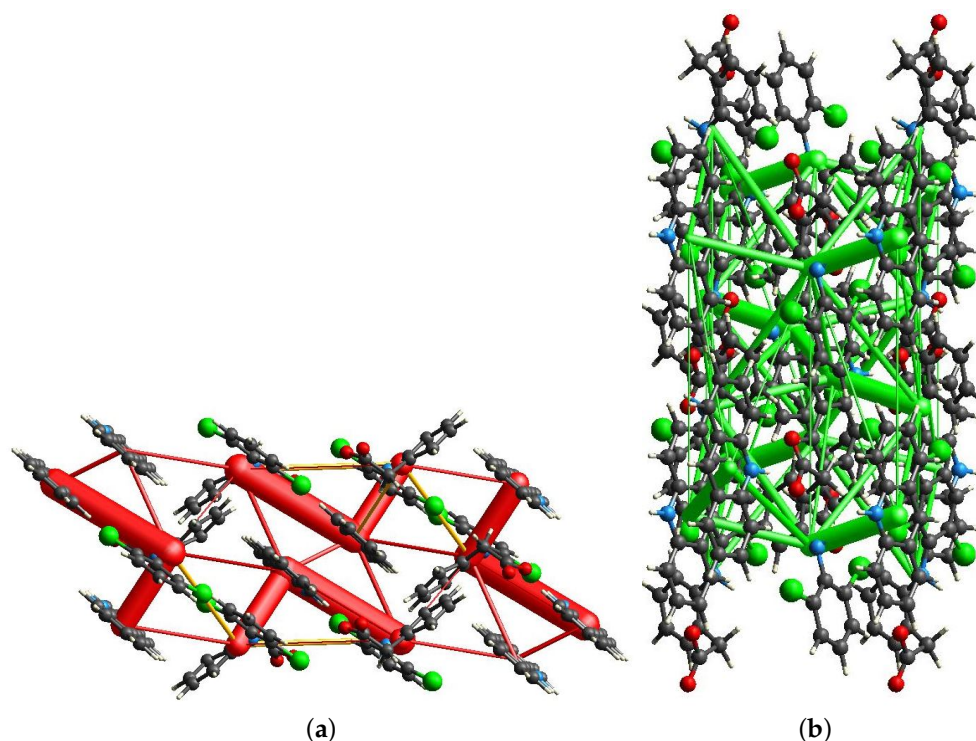


**Figure 8.** Energy frameworks calculated for salt form of the 1:1 LAG crystal structure. (a) Coulomb energy framework along the b-axis. (b) Dispersive energy framework along the a-axis.

#### 4. Conclusions

A new crystal structure was obtained using a mechanochemical approach (liquid assisted grinding), starting from acridine and diclofenac in a 1:1 ratio. The diffraction

data demonstrate a yield greater than 90% with a minimum waste of solvents and energy. The cocrystal structure was solved from powder diffraction data by simulated annealing and was analyzed by calculating the Hirshfeld surfaces and the energy frameworks. The same calculations were carried out for the 1:2 structure recently reported in the literature obtained by crystallization from solution and with a acridine/diclofenac ratio of 1:2. The 1:1 new structure shows a strong hydrogen bond and a cage-like structure. DSC analysis confirmed a melting point of the cocrystal at about 140 °C, which is different from those of the reactants (about 100 °C and about 284 °C for acridine and diclofenac, respectively). The 1:2 structure is the most stable cocrystal, probably because the packing of the 1:1 structure is stabilized only by one H-bond. Conversely, the previously identified cocrystal shows a perfect interlocking of the molecules, thanks to a net of strong H-bonds and extended  $\pi \cdots \pi$  stacking, which can explain its much larger stability, suggested by energy framework calculations. Although the 1:2 ratio structure is the most stable according to energy framework calculations, attempts at converting the 1:1 cocrystal presented in this paper to 1:2 have been unsuccessful. Additionally, LAG treatment of the reactants in 1:2 ratio converged to the production of a 1:1 product. The obtained product is thus strongly related to the preparation method (LAG or solution crystallization). Further experiments to verify the stability of the two species are not feasible because of the low quantities and low purity of the 1:2 product obtained via the solution crystallization process. The crystallographic data of a new structure have been uploaded to the CCDC website and correspond to the identification number 2211637.

**Author Contributions:** Conceptualization, A.S. and M.M.; data curation, E.C., L.P. and M.L.; formal analysis, A.M. and M.L.; funding acquisition, A.S. and M.M.; investigation, A.M.; methodology, A.M., E.C., L.P. and M.L.; validation, E.C. and L.P.; writing—original draft, M.M. and M.L.; writing—review and editing, A.M., E.C., L.P. and A.S. All authors have read and agreed to the published version of the manuscript.

**Funding:** The authors acknowledge the Research of Young Scientists grant (BMN) no. 539-T080-B027-22 (University of Gdansk), DS no. 531-T080-D738-22 (University of Gdansk), Project 288-105 by FINPIEMONTE within the Programma Pluriennale Attività Produttive 2015/2017 Misura 3.1 “Contratto d’insediamento” (Università del Piemonte Orientale).

**Data Availability Statement:** Data are contained within the article.

**Conflicts of Interest:** The authors declare no conflict of interest.

## References

1. Mirocki, A.; Lopresti, M.; Palin, L.; Conterposito, E.; Sikorski, A.; Milanesio, M. Exploring the molecular landscape of multicomponent crystals formed by naproxen drug and acridines. *CrystEngComm* **2022**, *24*, 6839–6853. [[CrossRef](#)]
2. Zaworotko, M. Crystal engineering of the composition of API's: Understanding polymorphs and designing pharmaceutical co-crystals. *Am. Pharm. Outsourcing* **2004**, *5*, 16–23.
3. Barbas, R.; Bofill, L.; de Sande, D.; Font-Bardia, M.; Prohens, R. Crystal engineering of nutraceutical phytosterols: New cocrystal solid solutions. *CrystEngComm* **2020**, *22*, 4210–4214. [[CrossRef](#)]
4. Qiao, N.; Li, M.; Schlindwein, W.; Malek, N.; Davies, A.; Trappitt, G. Pharmaceutical cocrystals: An overview. *Int. J. Pharm.* **2011**, *419*, 1–11. [[CrossRef](#)] [[PubMed](#)]
5. Desiraju, G. Crystal Engineering: A Holistic View. *Angew. Chem. Int. Ed.* **2007**, *46*, 8342–8356. [[CrossRef](#)]
6. Bhowal, R.; Biswas, S.; Thumbarathil, A.; Koner, A.L.; Chopra, D. Exploring the Relationship between Intermolecular Interactions and Solid-State Photophysical Properties of Organic Co-Crystals. *J. Phys. Chem. C* **2018**, *123*, 9311–9322. [[CrossRef](#)]
7. Walsh, R.D.B.; Bradner, M.W.; Fleischman, S.; Morales, L.A.; Moulton, B.; Rodríguez-Hornedo, N.; Zaworotko, M.J. Crystal engineering of the composition of pharmaceutical phases. *Chem. Commun.* **2002**, *2*, 186–187. [[CrossRef](#)]
8. Singh, G.; Fort, J.G.; Goldstein, J.L.; Levy, R.A.; Hanrahan, P.S.; Bello, A.E.; Andrade-Ortega, L.; Wallemark, C.; Agrawal, N.M.; Eisen, G.M.; et al. Celecoxib Versus Naproxen and Diclofenac in Osteoarthritis Patients: SUCCESS-I Study. *Am. J. Med.* **2006**, *119*, 255–266. [[CrossRef](#)]
9. Brogden, R.; Heel, R.; Pakes, G.; Speight, T.; Avery, G. Diclofenac Sodium. *Drugs* **1980**, *20*, 24–48. [[CrossRef](#)]
10. Goh, C.F.; Lane, M.E. Formulation of diclofenac for dermal delivery. *Int. J. Pharm.* **2014**, *473*, 607–616. [[CrossRef](#)]
11. Mazumdar, K.; Dastidar, S.G.; Park, J.H.; Dutta, N.K. The anti-inflammatory non-antibiotic helper compound diclofenac: An antibacterial drug target. *Eur. J. Clin. Microbiol. Infect. Dis.* **2009**, *28*, 881–891. [[CrossRef](#)]

12. Maitra, A.; Bates, S.; Shaik, M.; Evangelopoulos, D.; Abubakar, I.; McHugh, T.D.; Lipman, M.; Bhakta, S. Repurposing drugs for treatment of tuberculosis: A role for non-steroidal anti-inflammatory drugs. *Br. Med. Bull.* **2016**, *118*, 138–148. [[CrossRef](#)]
13. Kroesen, V.M.; Gröschel, M.I.; Martinson, N.; Zumla, A.; Maeurer, M.; van der Werf, T.S.; Vilaplana, C. Non-Steroidal Anti-inflammatory Drugs As Host-Directed Therapy for Tuberculosis: A Systematic Review. *Front. Immunol.* **2017**, *8*. [[CrossRef](#)]
14. Todd, P.A.; Sorkin, E.M. Diclofenac Sodium. *Drugs* **1988**, *35*, 244–285. [[CrossRef](#)]
15. Groom, C.R.; Bruno, I.J.; Lightfoot, M.P.; Ward, S.C. The Cambridge Structural Database. *Acta Crystallogr. Sect. B Struct. Sci. Cryst. Eng. Mater.* **2016**, *72*, 171–179. [[CrossRef](#)]
16. Aakeröy, C.B.; Grommet, A.B.; Desper, J. Co-Crystal Screening of Diclofenac. *Pharmaceutics* **2011**, *3*, 601–614. [[CrossRef](#)]
17. Bodart, L.; Prinzo, M.; Derlet, A.; Tumanov, N.; Wouters, J. Taking advantage of solvate formation to modulate drug–drug ratio in clofaziminium diclofenac salts. *CrystEngComm* **2021**, *23*, 185–201. [[CrossRef](#)]
18. Bhattacharya, B.; Mondal, A.; Soni, S.R.; Das, S.; Bhunia, S.; Raju, K.B.; Ghosh, A.; Reddy, C.M. Multidrug salt forms of norfloxacin with non-steroidal anti-inflammatory drugs: Solubility and membrane permeability studies. *CrystEngComm* **2018**, *20*, 6420–6429. [[CrossRef](#)]
19. Surov, A.O.; Voronin, A.P.; Vener, M.V.; Churakov, A.V.; Perlovich, G.L. Specific features of supramolecular organisation and hydrogen bonding in proline cocrystals: A case study of fenamates and diclofenac. *CrystEngComm* **2018**, *20*, 6970–6981. [[CrossRef](#)]
20. Nugrahani, I.; Kumalasari, R.A.; Auli, W.N.; Horikawa, A.; Uekusa, H. Salt Cocrystal of Diclofenac Sodium-L-Proline: Structural, Pseudopolymorphism, and Pharmaceutics Performance Study. *Pharmaceutics* **2020**, *12*, 690. [[CrossRef](#)]
21. Wang, R.; Yuan, P.; Yang, D.; Zhang, B.; Zhang, L.; Lu, Y.; Du, G. Structural features and interactions of new sulfamethazine salt and cocrystal. *J. Mol. Struct.* **2021**, *1229*, 129596. [[CrossRef](#)]
22. Mirocki, A.; Sikorski, A. Structural Characterization of Multicomponent Crystals Formed from Diclofenac and Acridines. *Materials* **2022**, *15*, 1518. [[CrossRef](#)] [[PubMed](#)]
23. Karimi-Jafari, M.; Padrela, L.; Walker, G.M.; Croker, D.M. Creating Cocrystals: A Review of Pharmaceutical Cocrystal Preparation Routes and Applications. *Cryst. Growth Des.* **2018**, *18*, 6370–6387. [[CrossRef](#)]
24. Braga, D.; Casali, L.; Grepioni, F. The Relevance of Crystal Forms in the Pharmaceutical Field: Sword of Damocles or Innovation Tools? *Int. J. Mol. Sci.* **2022**, *23*, 9013. [[CrossRef](#)] [[PubMed](#)]
25. Acebedo-Martínez, F.J.; Alarcón-Payer, C.; Barrales-Ruiz, H.M.; Niclós-Gutiérrez, J.; Domínguez-Martín, A.; Choquesillo-Lazarte, D. Towards the Development of Novel Diclofenac Multicomponent Pharmaceutical Solids. *Crystals* **2022**, *12*, 1038. [[CrossRef](#)]
26. Saikia, B.; Pathak, D.; Sarma, B. Variable stoichiometry cocrystals: Occurrence and significance. *CrystEngComm* **2021**, *23*, 4583–4606. [[CrossRef](#)]
27. Losev, E.A.; Boldyreva, E.V. A salt or a co-crystal – when crystallization protocol matters. *CrystEngComm* **2018**, *20*, 2299–2305. [[CrossRef](#)]
28. Altomare, A.; Cuocci, C.; Giacovazzo, C.; Moliterni, A.; Rizzi, R.; Corriero, N.; Falcicchio, A. EXPO2013: A kit of tools for phasing crystal structures from powder data. *J. Appl. Crystallogr.* **2013**, *46*, 1231–1235. [[CrossRef](#)]
29. Coelho, A. TOPAS and TOPAS-Academic : An optimization program integrating computer algebra and crystallographic objects written in C++. *J. Appl. Crystallogr.* **2018**, *51*. [[CrossRef](#)]
30. Coelho, A. *TOPAS-Academic V7*; Coelho Software: Brisbane, Australia, 2020.
31. Lopresti, M.; Mangolini, B.; Milanesio, M.; Caliendo, R.; Palin, L. Multivariate versus traditional quantitative phase analysis of X-ray powder diffraction and fluorescence data of mixtures showing preferred orientation and microabsorption. *J. Appl. Crystallogr.* **2022**, *55*, 837–850. [[CrossRef](#)]
32. Mackenzie, C.F.; Spackman, P.R.; Jayatilaka, D.; Spackman, M.A. CrystalExplorer model energies and energy frameworks: Extension to metal coordination compounds, organic salts, solvates and open-shell systems. *IUCr* **2017**, *4*, 575–587. [[CrossRef](#)]
33. Jayatilaka, D.; Grimwood, D.J. Tonto: A Fortran Based Object-Oriented System for Quantum Chemistry and Crystallography. In *Computational Science—ICCS 2003, Proceedings of the International Conference, Melbourne, Australia and St. Petersburg, Russia, 2–4 June 2003*; Lecture Notes in Computer Science; Springer: Berlin/Heidelberg, Germany, 2003; pp. 142–151. [[CrossRef](#)]
34. Thomas, S.P.; Spackman, P.R.; Jayatilaka, D.; Spackman, M.A. Accurate Lattice Energies for Molecular Crystals from Experimental Crystal Structures. *J. Chem. Theory Comput.* **2018**, *14*, 1614–1623. [[CrossRef](#)]
35. Macrae, C.F.; Sovago, I.; Cottrell, S.J.; Galek, P.T.A.; McCabe, P.; Pidcock, E.; Platings, M.; Shields, G.P.; Stevens, J.S.; Towler, M.; et al. Mercury 4.0: From visualization to analysis, design and prediction. *J. Appl. Crystallogr.* **2020**, *53*, 226–235. [[CrossRef](#)]
36. Majerz, I.; Gutmann, M.J. Intermolecular OHN hydrogen bond with a proton moving in 3-methylpyridinium 2, 6-dichloro-4-nitrophenolate. *RSC Adv.* **2015**, *5*, 95576–95584. [[CrossRef](#)]
37. Socrates, G. *Infrared and Raman Characteristic Group Frequencies*; John Wiley & Sons: Hoboken, NJ, USA, 2004.
38. Lide, D.R. *CRC Handbook of Chemistry and Physics*, 90th ed.; CRC Press: Boca Raton, FL, USA, 2009.